Article

A Novel Electrochemiluminescence Peptide-Based Biosensor with Hetero-Nanostructures as Co-reaction Accelerator for the Ultra-sensitive Determination of Tryptase

Fang-Fang Wu, Ying Zhou, Han Zhang, Ruo Yuan, and Ya-Qin Chai

Anal. Chem., **Just Accepted Manuscript** • DOI: 10.1021/acs.analchem.7b04631 • Publication Date (Web): 27 Dec 2017

A Novel Electrochemiluminescence Peptide-Based Biosensor with Hetero-Nanostructures as Co-reaction Accelerator for the Ultra-sensitive Determination of Tryptase

Fang-Fang Wu, Ying Zhou, Han Zhang, Ruo Yuan, Ya-Qin Chai**

Key Laboratory of Luminescent and Real-Time Analytical Chemistry (Southwest University), Ministry of Education, College of Chemistry and Chemical Engineering, Southwest University, Chongqing 400715, PR China

*Corresponding author. Tel.: +86-23-68252277; Fax: +86-23-68253172

E-mail address: yuanruo@swu.edu.cn, yqchai@swu.edu.cn.

ABSTRACT: In this work, a luminol-centric biosensor was constructed for the ultrasensitive detection of tryptase (TPS) combining dissolved O_2 as the endogenous coreactant and Au-Ag-Pt hetero-nanostructures (AAPHNs) as co-reaction accelerator. Dissolved O_2 could rapidly generate superoxide anion radical ($O_2^{\bullet-}$) with the catalysis of AAPHNs to in situ react with luminol anion radical ($L^{\bullet-}$) to generate excited-state species 3-aminophthalate (AP^{2-*}) for emitting ECL signal, resulting in a remarkable "single on" state. In order to further improve the sensitivity of the sensor, we employed self-assembled DNA nanotubes (DNANTs) as a carrier to immobilize the luminophore of doxorubicin-luminol (Dox-Lu) complex. In this assay system, target tryptase could directly induce the cleavage of vasoactive intestinal peptide (VIP), which caused the ECL probe of DNANTs-Dox-Lu releasing from the electrode surface to obtain a significant "signal off" state. By changing the signal from "on" to "off", the proposed ECL peptide-based biosensor for TPS detection achieved a dynamic concentration range (2.5 pg/mL-200 ng/mL) with an extremely low detection limit of 0.81 pg/mL. This work presented a new signal amplification method for the construction of the sensor based on the luminol-dissolved O_2 ECL system.

KEYWORDS: Au-Ag-Pt hetero-nanostructures, luminol-dissolved oxygen system, electrochemiluminescence (ECL), peptide

INTRODUCTION

Electrochemiluminescent (ECL), as a powerful analytical method, has been paid greatly attention in recent years.[1-3] It was widely used in various fields such as environmental pollutant monitoring, drug analysis and human related biomolecules detection because of its low background, wide dynamic range and high sensitivity.[4,5] Luminol as a typical ECL luminophore was widely used in biosensors.[6-8] Usually, H_2O_2 was used as the co-reactant to enhance the luminous intensity of luminol for

improving the sensitivity of the biosensor.[9-11] Whereas, H_2O_2 was harmful to biology,[12] therefore the development of H_2O_2-free strategy to enhance the ECL performance of luminol-centric biosensor was of great importance. Compared with H_2O_2, the non-toxic co-reactant of dissolved O_2 could be a desirable candidate to apply in biosensors fabrication. Nevertheless, the reaction efficiency of luminol-O_2 system was too low to afford a remarkable signal amplification, thus hindering the widespread application of the luminol-O_2 system. So it was meaningful to improve the efficiency of the interaction between luminol and dissolved O_2.

The co-reaction accelerator was a species that when it was introduced into the ECL system containing luminophore and co-reactant, it could affect the co-reactant rather than luminophore to promote the ECL reaction rate of luminophore and co-reactant, thus the ECL signal was significantly amplified in comparison with that in which only luminophore and co-reactant were present. Recently, our group introduced semicarbazide as a co-reaction accelerator to significantly enhance the efficiency of the interaction between CdTe QDs and $S_2O_8^{2-}$.[13] In this paper, Au-Ag-Pt hetero-nanostructures (AAPHNs) were used as a new co-reaction accelerator to improve the efficiency of the interaction between luminol and dissolve O_2 to construct highly sensitive ECL biosensor.

Precious metal nanomaterials such as Au, Ag, and Pt were widely used in the ECL biosensors because of their excellent electrical conductivity, biocompatibility and electrocatalytic activity.[14-16] Au-Ag-Pt hetero-nanostructures (AAPHNs), as a kind of multifunctional nanomaterials combined the properties of the three precious metals with distinctive geometrical shape was reported in the previous literature.[17] Pt was a key element for catalysis in both anodes and cathodes, and AAPHNs exhibited higher catalytic activity compared with Pt itself owing to the synergistic effects of Au, Ag

and Pt. In this work, the AAPHNs were firstly used as an ECL co-reaction accelerator to effectively promote the reduction of dissolved O_2 to generate $O_2^{\bullet-}$ to in situ react with the luminol anion radical ($L^{\bullet-}$) to produce excited-state species 3-aminophthalate (AP^{2-*}) for emitting ECL signal, resulting in a strong ECL signal (Scheme 1C).

Tryptase (TPS) as a specific protease released during the allergic process, and could specifically crack vasoactive intestinal peptide[18] (VIP), which was a useful indicator of clinical evaluation of allergic diseases.[19-21] Usually, the TPS concentration in normal serum was under 5 ng/mL,[22] which was too low to detect. Herein, we developed a novel ECL peptide-based biosensor for sensitive detection of TPS based on target-induced cleavage of specific peptide in luminol-dissolved O_2 ECL system. First, luminol was significantly immobilized on self-assembled DNA nanotubes (DNANTs) with the form of doxorubicin-luminol (Dox-Lu) complex, due to double-stranded insertability of Dox. The sensing interface was obtained by progressively assembling AAPHNs and DNA nanotube-Dox-luminol (DNANTs-Dox-Lu) labeled vasoactive intestinal peptide (VIP-DNANTs-Dox-Lu) on the glassy carbon electrode surface to obtain the potent ECL signal. Since the target TPS specifically cleaved VIP (The structure and cleavage site of the peptide were shown in the Supplementary Information), DNANTs-Dox-Lu and partial peptides were released from the electrode surface, resulting in a prominent reduction of ECL intensity as the "signal off" state. This proposed ECL peptide-based biosensor exhibited a wide linear range (2.5 pg/mL-200 ng/mL) and a low detection limit (0.81 pg/mL), which was expected to be an effective method for clinical and forensic detection of TPS.

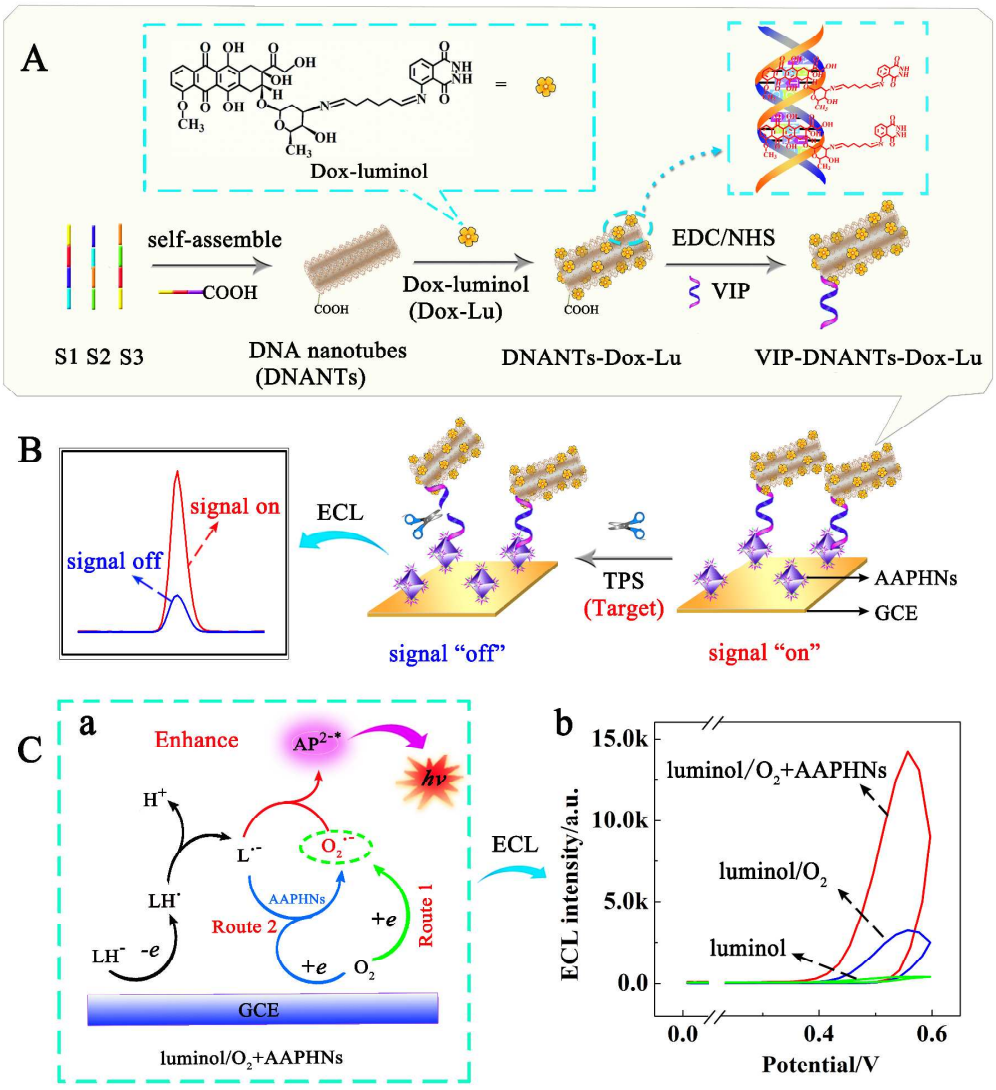

Scheme 1. Schematic diagram showing (A) the preparation of VIP-DNA nanotubes-Dox-luminol indecator, (B) the ECL peptide-based biosensor fabrication process. (C) The possible (a) ECL mechanism of the luminol/O_2+AAPHNs ECL system and (b) ECL responses of luminol, luminol/O_2 and luminol/O_2+AAPHNs.

EXPERIMENTAL SECTION

Chemicals and Materials. Silver nitrate ($AgNO_3$, 99.9%), cetyltrimethylammonium bromide (CTAB, ≥99%), L-ascorbic acid (AA, 99.98%), sodium borohydride ($NaBH_4$) were purchased from Chengdu Kelong Chemical

Industry (Chengdu, China). Luminol (98%), gold chloride ($HAuCl_4 \cdot 4H_2O$, 99.9%) and doxorubicin hydrochloride (Dox) were obtained from Sigma-Aldrich Co. (St. Louis, MO, U.S.A.). Glutaraldehyde (GA) was supplied by Shanghai Medpep Co. Ltd. (Shanghai, China). Potassium tetrachchloroplainate (II) (K_2PtCl_4, 99.95%, J&K) was purchased from Kangda Amino Acid Company (Shanghai, China). Vasoactive intestinal peptide (VIP) was supplied by Nanjing Peptide Biotech Ltd. (Nanjing, China). Tryptase (TPS) was obtained from Shanghai Jingkang Biological Engineering Co., Ltd (Shanghai, China). All the synthetic DNA sequences employed in this work (displayed in Table S1) were purchased from Shanghai Sangon Biological Engineering Technology & Services Co., Ltd. (Shanghai, China) with PAGE purification. The human serum samples were provided by Chongqing Municipal People's Hospital (Chongqing, China). Phosphate-buffered solution (PBS, 0.1 M, containing 2 mM $MgCl_2$ and 10 mM KCl, pH 8.0) was employed as the working buffer solution. Tris-acetate-EDTA buffer (TAE, containing 20 mM Tris, 2 mM EDTA, 10 mM $MgCl_2$, pH 8.0) was employed as the binding buffer. Ultrapure water (specific resistance of 18.2 MΩ·cm) was used throughout this experiment.

Apparatus. ECL signals were monitored and recorded by a model *MPI-E* ECL analyzer (Xi'an Remax Electronic Science & Technology Co. Ltd., Xi'An, China) with the voltage of the photomultiplier tube (PTM) set at 800 V and the potential scan from 0 to 0.6 V in the process of detection. The entire experimental tests were performed at room temperature using a three-electrode system, which was formed with the modified glass carbon electrode (GCE, Φ = 4 mm) as the working electrode, saturated calomel electrode (SCE) or Ag/AgCl (sat. KCl saturated solution) as the reference electrode and a platinum wire as counter electrode during ECL detection. The cyclic voltammetry (CV) measurements were performed with a CHI 660A

electrochemical workstation (Shanghai Chenhua Instrument, China). The UV-vis absorption spectra were captured and recorded on a UV-2450 spectrophotometer (Shimadzu, Tykyo, Japan). The morphology of AuNRs was characterized by scanning electron microscopy (SEM, S-4800, Hitachi, Tokyo, Japan) with a voltage of 20-30 kV. The structures of AAPHNs were confirmed by a transmission electron microscope (TEM, H600, Hitachi Instrument, Japan) and the constituent elements of AAPHNs were characterized by energy dispersive spectrometer (EDS, TECAI G2F20, Hitachi Instrument, Japan).

Preparation of AuNRs and Au-Ag-Pt Hetero-nanostructures (AAPHNs). The preparation of AuNRs used a seed-mediated growth method, according to the previous literature[23,24] with a minor modification. (1) Seed solution: 5.00 mL of 0.2 M CTAB solution was mixed with 0.25 mL of 10 mM $HAuCl_4$ and 4.75 mL of ultrapure water, and 0.60 mL of 10 mM ice-cooled $NaBH_4$ was added while stirring the solution. Then, the above solution was strongly stirred for 2 min. After that, it was keep at room temperature for 3 h. (2) AuNRs Growth: CTAB solution (5.00 mL, 0.2 M) was added to 0.20 mL of 10 mM $AgNO_3$ and 4.30 mL of ultrapure water. 0.50 mL of 10 mM $HAuCl_4$ was added into the above solution, and after gentle mixing, 70 μL of 0.08 M AA was injected with mild stirring. Finally, 12 μL of Au seed was added into the growth solution, and stired at 30 ^oC for 12 h.

The preparation process of AAPHNs was shown schematically in Figure S1 according to the previous literature.[14] Briefly, 8.60 mL of ultrapure water, 0.10 mL of 10 mM $AgNO_3$, 0.10 mL of 10 mM $HAuCl_4$ and 0.10 mL of 10 mM K_2PtCl_4 were sequentially added into a 20 mL bottle, then 1.00 mL of Au nanorods solution and 0.30 mL of 0.08 M AA were added into above mixture with magnetic stirring. After reacted at room temperature for 16 h, the product was collected by centrifugation at

12000 rpm for 10 min, washed by ultrapure water for several times to removal excess CTAB.

Preparation of the Doxorubicin hydrochloride-luminol (Dox-Lu) Compounds. The preparation of Dox-Lu compounds were showed schematically in Scheme 1(A). Firstly, luminol solution (0.50 mL, 1 mM) was mixed with Dox solution (0.50 mL, 15 mM) through ultrasonication. Subsequently, glutaraldehyde (GA, 0.50 mL, 1 %) as cross-linking agent, was added into the mixture solution mentioned above with constant stirring for 24 h to obtain the Dox-Lu compounds.

Preparation of DNA Nanotubes-Doxorubicin hydrochloride-Luminol (DNANTs-Dox-Lu) Complex and VIP-DNA Nanotubes-Doxorubicin hydrochloride-Luminol (VIP-DNANTs-Dox-Lu) Complex. The carboxyl modified DNA nanotubes (DNANTs) were obtained according to the literature[25] with a minor modification. Three types of brick SSTs monomers S1, S2 and S3 (the corresponding sequence structures were shown in Table S1) were used to construct the nanotubes by a one-pot annealing from 95 ^{o}C to room temperature in the Tris-acetate-EDTA (TAE) buffer with a final concentration of 1 μM for each strand. The proportions of the three standard chains of S1, S2 and S3 were the same. Followed by the addition of R1, a carboxyl-modified single-stranded DNA was complementary to a portion of the S1 strand to construct the carboxy-modified DNA nanotube.

After successful assembly of the DNA nanotubes, 1 mL of the prepared Dox-Lu compounds were added into the above DNA nanotubes and stored for 4 h to embed Dox-Lu in double-stranded structures of DNA nanotubes. Subsequently, the above mixture was transferred into a dialysis tube containing 100 mL of PBS to dialyze for 1 day with slight shaking to obtain DNA nanotubes-Dox-luminol (DNANTs-Dox-Lu) complex. After that, the carboxyl groups modified DNANTs-Dox-Lu complex could

be easily bound to the surface of the amino-rich VIP peptide *via* amide bond. Briefly, 0.4 mg VIP was dissolved in 1.00 mL PBS (10 mM, pH 7.4) and then mixed with 2.00 mL as-prepared DNANTs-Dox-Lu complex, and finally a mixed solution of 10 μL EDC (20 mg) and NHS (10 mg) was added into the composite and continuously stirring for 8 h at 4 ^{o}C. After centrifugated for 5 min at 3000 rpm, the lower products (VIP-DNANTs-Dox-Lu) were collected for later use.

Fabrication of the ECL peptide-based biosensor. Glassy carbon electrode (GCE, Φ = 4) was polished repeatedly with 0.3 and 0.05 μm alumina powder, followed by ultrasonic cleaning with ultrapure water and alcohol, respectively. Subsequently, 10 μL AAPHNs nanocomplex was dripped onto the electrode surface by a microsyringe and then it was naturally dried in air at room temperature to obtain AAPHNs modified GCE (AAPHNs/GCE). After that, 15 μL of VIP-DNANTs-Dox-Lu was added onto the above modified electrode surface and incubated at 4 ^{o}C for 8 h to form an ECL layer of VIP-DNANTs-Dox-Lu/AAPHNs/GCE. After rinsing the unlinked VIP-DNANTs-Dox-Lu with 0.1 M PBS buffer (pH 8.0), the modified electrode was immersed in 1 wt% BSA solution at 37 ^{o}C for 20 min to block the remaining active sites. Each step of the sensor interface modifications was characterized by cyclic voltammetry in 5.0 mM $[Fe(CN)_6]^{3-/4-}$ solution and the results were shown in Figure S2, and the sensor construction process was shown in Scheme 1B.

Measurement procedure. The fabricated ECL peptide-based biosensor was immersed in a series of different standard concentrations of TPS solutions dissolved in PBS or serum and incubated at 37 °C for 40 minutes, followed by washing with 0.1 M PBS (pH 8.0). The ECL measurements were performed in 0.1 M PBS (2.0 mL, pH 8.0) with a continuous cyclic potential scan from 0 to 0.6 V. The concentration of TPS can be quantified by the decreased ECL intensity ($\Delta E = E_0 - E_s$, where E_s and E_0

represent the ECL intensity of the ECL peptide-based biosensor with or without TPS incubated, respectively).

RESULTS AND DISSCUSSION

Characterization of AuNRs and Au-Ag-Pt Hetero-nanostructures (AAPHNs). As shown in Figure 1A, the synthetic AuNRs exhibited a highly uniform morphology with about 30 nm long and 10 nm wide, which was consistent with the literatures.[26,27] As seen from Figure 1B, AAPHNs exhibited a typical multiple heterostructures and distinctive geometrical shape: a Au nanorod core of the interior, a Au/Ag octahedron shell for the exterior, and dendritic Ag/Pt alloys decorated onto the vertices. High resolution transmission electron microscopy (HRTEM) images Figure 1B clearly revealed that the main octahedral structure was approximately 70 nm, and the dendritic Ag/Pt alloys decorated onto the vertices were nearly 5 nm. Moreover, EDS characterization was employed for elemental analysis of AAPHNs. As can be seen from Figure 1D, the presence of Au (2.123 keV, 2.41 keV, 8.494 keV, 9.713 keV), Ag (2.634 keV, 2.806 keV, 2.984 keV, 3.151 keV) and Pt (1.592 keV, 2.331 keV, 2.05 keV, 8.268 keV, 9.442 keV, 9.975 keV) elements verified the existence composition of the AAPHNs. This hetero-nanostructure was easy to adsorb free radical ions due to its precious metal nanoparticles containing Au, Ag and Pt[28]. In addition, the prepared AAPHNs exhibited good film-forming properties, which was advantageous to fabricate the modified electrode. The curve a and curve b in Figure 1C showed the UV absorption spectra of the synthesized AuNRs and AAPHNs, which were consistent with the data provided by the Cai group[17], thus further demonstrating the successful preparation of the alloy.

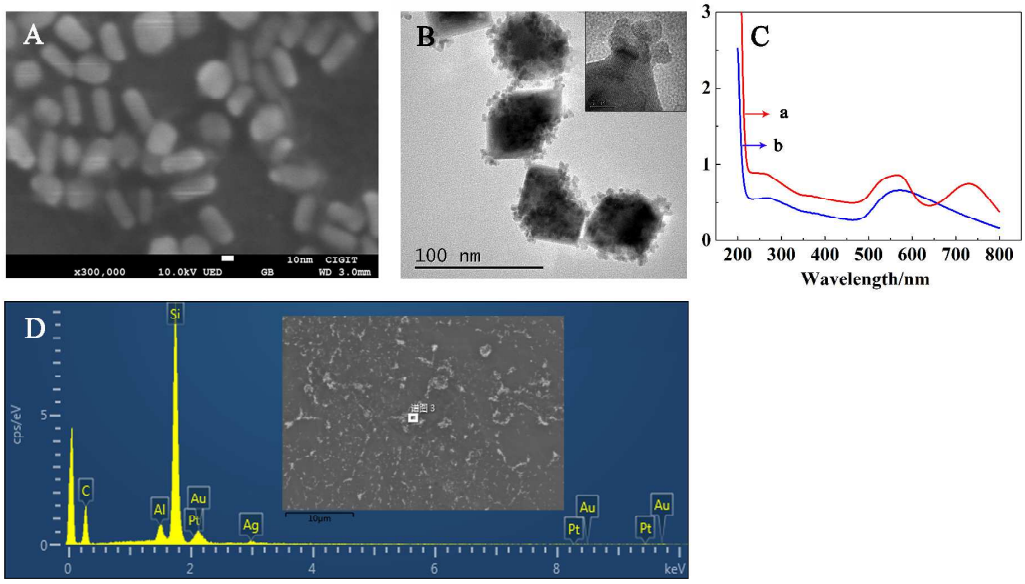

Figure 1. (A) SEM image of AuNRs. (B) HRTEM image of AAPHNs. The inset of panel (B) showed a partially enlarged HRTEM image of the dendritic Ag/Pt alloys decorated onto the vertices. (C) UV-vis spectrums of (a) AuNRs; (b)Au-Ag-Pt hetero-nanostructure. (D) EDS pattern of AAPHNs.

Characterization of Dox-Lu compounds. The preparation of Dox-Lu compounds was clearly shown in Figure 2A. Simultaneously, the UV-vis absorption spectra was performed to confirm the synthesis of Dox-Lu compounds directly. Figure 2B showed the UV-vis absorbance spectra for each ingredient (Dox, luminol, and Dox-Lu compounds). Luminol had two characteristic absorption peaks at 300 nm and 349.5 nm (curve a), and the absorption spectra of Dox-Lu compounds depending on a new absorption band appeared at 480.5 nm (curve c), which was associated with the Dox (curve b). Furthermore, the peak at 230 nm in the UV-vis absorbance spectrums of both Dox and luminol, which ascribed to the UV absorption of $-NH_2$, were disappeared in the Dox-Lu compounds because the cross-linking agent GA consumed their $-NH_2$ group. The results indicating that Dox-Lu compound was successfully synthesized.

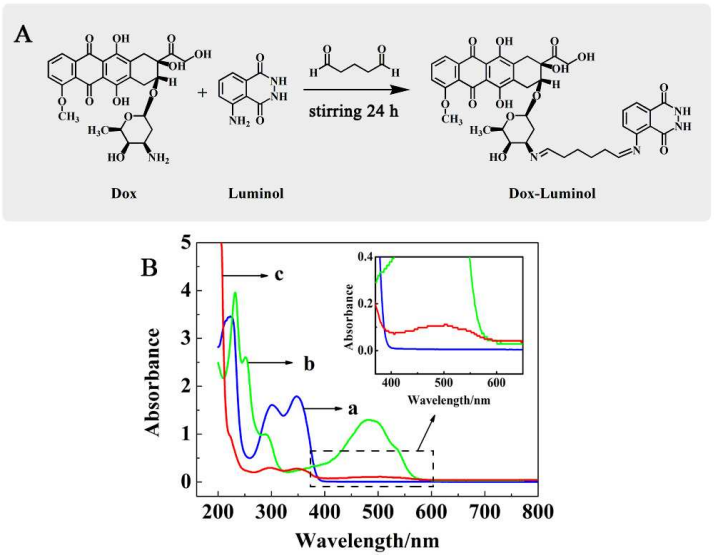

Figure 2. (A) Synthetic route of the Dox-luminol compounds. (B) UV-vis spectrum of (a) luminol; (b) Dox; (c) Dox-luminol compounds.

Characterization of DNA nanotubes. The prepared DNA nanotubes were characterized by agarose gel electrophoresis. As shown in Figure 3, the single strand DNA of R1 with the lowest molecular weight was run fastest on the agarose gel (lane 4). As expected, S1, S2 and S3, three bright bands at a similar position were observed (lane 1−3), due to their similar molecular weight. Moreover, after the single strand DNA (S1, S2, S3 and R1) self-assembled into the target DNA nanotubes, the DNA nanotubes with highest molecular weight run slowest (lane 5). The above results demonstrated the successful formation of the DNA nanotubes.

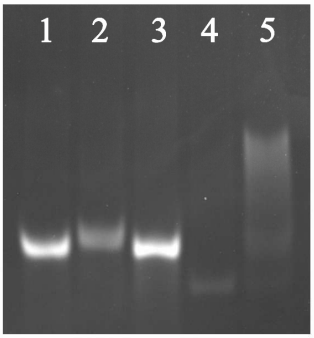

Figure 3. Agarose gel electrophoresis characterization of different DNA nanostructure: lane 1, S1; lane 2, S2; lane 3, S3; lane 4, R1; lane 5, DNA nanotubes.

DNA nanotubes immobilized luminol. To illustrate that DNA nanotubes can efficiently immobilize luminol, we compared ECL responses in three different conditions and the corresponding results were presented in Figure 4. As can be seen from the Figure 4A, due to the lack of luminescent reagents, there was almost no ECL response when DNA nanotubes (DNANTs) was directly dropped in the modified electrode (VIP/AAPHNs/GCE). Subsequently, a weak ECL signal of about 823 a.u (Figure 4B) was obtained when the modified electrode (VIP/AAPHNs/GCE) was immersed in Dox-Lu. It was probably due to a small fraction of luminescent molecules (Dox-Lu) adsorbed to the electrode surface. However, when DNANTs-Dox-Lu (Figure 4C) was incubated into the modified electrode (VIP/AAPHNs/GCE) surface, the ECL intensity was prominently increased from 823 a.u to 13087 a.u (about 16-fold increase), indicating that DNA nanotubes could as a carrier to immobilize the luminophore of Dox-Lu and effectively increase the ECL intensity of the sensor.

In addition, we have showed the fabrication process of DNANTs-Dox-Lu (Figure 4D). It can be seen from the Figure 4D that the structure of DNA nanotubes were rich in DNA double-stranded structures. Dox was a good double-stranded intercalator,[29,30] so that luminophore (Dox-Lu) could be largely loaded onto DNA nanotubes through the interaction between the Dox and DNA double-stranded structures.

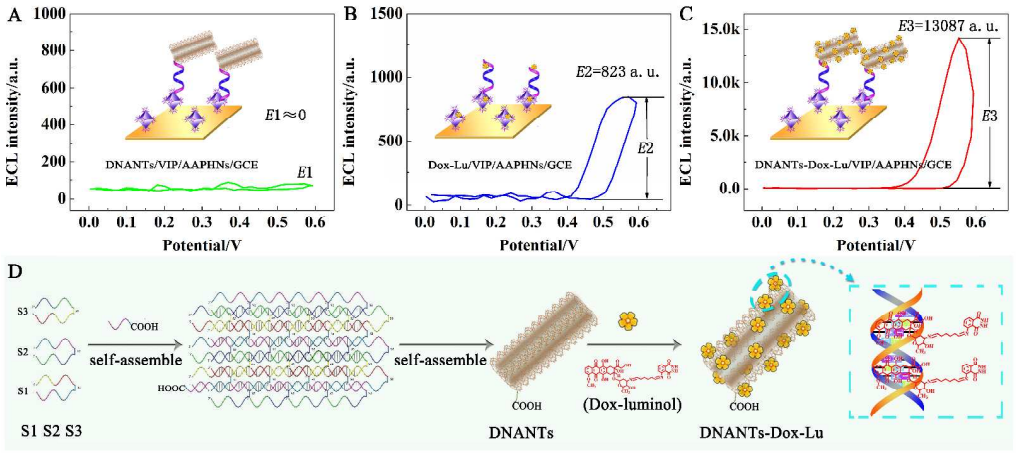

Figure 4. ECL responses of (A) DNANTs/VIP/AAPHNs/GCE, (B) Dox-Lu/VIP/AAPHNs/GCE and (C) DNANTs-Dox-Lu/VIP/AAPHNs/GCE. (D) The fabrication process of DNANTs-Dox-Lu.

Possible Luminescence Mechanism of Luminol-Dissolved O_2 ECL System. To investigate the possible luminescence mechanism of the ECL system, we compared the ECL and CV responses in four different solutions and the corresponding results were displayed in Figure 5. As can be seen from the Figure 5A, a ECL signal of about 300 a.u was obtained in N_2-saturated luminol solution (curve a) and it showed no noticeable change in comparison with that in the presence of AAPHNs (curve b), indicating that AAPHNs had no direct promotion on luminol. When the bare GCE was immersed in air-saturated luminol, the ECL signal was remarkably raised to 2565 a.u, revealing that dissolved O_2 as the co-reactant could improve the ECL emission of luminol. However, when AAPHNs was introduced into the luminol-O_2 ECL system (curve d), the ECL intensity was prominently increased from 2565 a.u to 15227 a.u (about 6-fold increase), meanwhile, the corresponding peak potential was negatively shifted from 0.43 V to 0.37 V. These revealed that AAPHNs as the co-reaction accelerator could actually make the ECL reaction of luminol and dissolved O_2 more efficient.

Meanwhile, the corresponding CV curves of the four different solutions were shown in Figure 5B. A distinctly anodic peak about 0.53 V (curve a) could be observed in the N_2-saturated luminol solution. After AAPHNs/GCE was immersed in the N_2-saturated luminol solution, the anodic current of the luminol was increased but the peak potential remained unchanged (curve b). This phenomenon further revealed that AAPHNs enhanced the conductivity of the GCE but didn't react directly with luminol. When the GCE was measured in air-saturated luminol solution, the anodic peak was shifted negatively from 0.53 V to 0.45 V (curve c) due to the decrease of the overpotential from the interaction between luminol and O_2. Furthermore, when AAPHNs/GCE was immersed in air-saturated luminol solution, the corresponding current was markedly enhanced (curve d), indicating that AAPHNs was indeed acted as the co-reaction accelerator to interact with O_2 for promoting the interaction between luminol and O_2.

Combining the reference[31-33] with our experimental results, the possible ECL mechanisms of luminol, luminol/O_2 and luminol/O_2+AAPHNs systems were shown in Figure 5C. Due to the lack of co-reaction reagents, luminol could not produce effective ECL emission (Figure 5Ca). In the luminol/O_2 system, O_2 on the GCE surface generated superoxide anion radical ($O_2^{\bullet-}$) and then reacted with luminol to produce ECL emission (Figure 5Cb). However, when AAPHNs was introduced into the luminol-O_2 ECL system, AAPHNs promoted the production of more $O_2^{\bullet-}$ (Figure 5Cc, route 1 and 2 : Route 1, electron exchange of O_2 on the GCE surface generate $O_2^{\bullet-}$; route 2, interaction between $L^{\bullet-}$ and O_2 on the AAPHNs/GCE surface generate $O_2^{\bullet-}$) that catalyzed luminol to produce significant ECL emission. In conclusion, the mechanism for luminol//O_2+AAPHNs systems could be described as follows:

$$LH^- - e^- \rightarrow L^{\bullet -} + H^+ \quad (1)$$

$$L^{\bullet -} + O_2 \xrightarrow{AAPHNs} O_2^{\bullet -} + L \quad (2)$$

$$L^{\bullet -} + O_2^{\bullet -} \rightarrow LO_2^{2-} \quad (3)$$

$$LO_2^{2-} \rightarrow AP^{2-*} + N_2 \quad (4)$$

$$AP^{2-*} \rightarrow AP^{2-} + h\nu \quad (5)$$

First of all, luminol anions (LH^-) were electrochemically oxidized to produce luminol anionic radicals ($L^{\bullet -}$). secondly, dissolved O_2 was aggregated on the interface of AAPHNs and rapidly reduced to $O_2^{\bullet -}$. And then the $O_2^{\bullet -}$ and the $L^{\bullet -}$ could in situ react on the surface of AAPHNs, which produce excited-state species AP^{2-*} for emitting ECL remarkably.

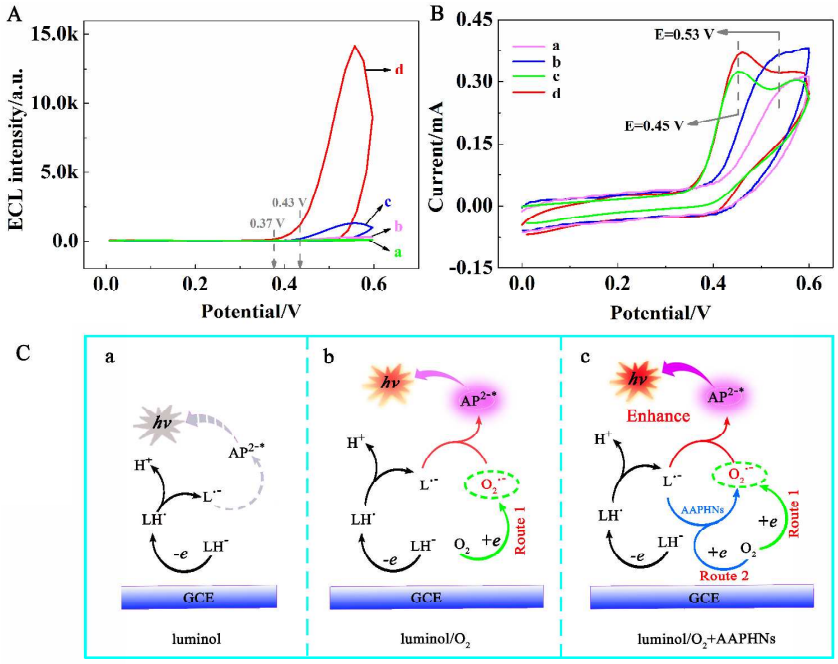

Figure 5. (A) ECL-potential and (B) cyclic voltammogram curves of GCE in (a) N_2-saturated luminol, (b) N_2-saturated luminol + AAPHNs (c) luminol/O_2 and (d) luminol/O_2 + AAPHNs. All the experiments were monitored in PBS (pH 8.0) with scan potential ranged from 0 to 0.6 V at a scan rate of 0.2 V/s. (C) The possible ECL mechanisms of (a) luminol, (b) luminol/O_2 and (c) luminol/O_2+AAPHNs systems.

Meanwhile, several related experiments were performed to explore the intrinsic mechanism of AAPHNs as co-reaction accelerator and the results were listed in Figure S3. As illustrated in Figure S3, the AAPHNs as a co-reaction accelerator made the obtained ECL signal higher and stabler compared to pure Au, Au-Ag and Au-Pt nanostructure in the detection system. It can be attributed to its typical multiple heterostructures and distinctive geometrical shape: Firstly, the unique trimetallic structures present plenty of Pt edge atoms on the surface as activated sites for oxygen oxidation.[34] In addition, the synergistic effect between Pt, Ag and Au could promote their catalytic performance.[17,35] Moreover, the metal nanoparticles could efficiently adsorbe radicals,[36] which shorten the distance of luminol radical and superoxide anion radical in ECL reaction, resulting in higher luminescent efficiency.

The Calibration Curve for TPS Detection. As shown in Figure 6, the decreased ECL intensity (ΔE) of ECL-PB sensors varies with different concentrations of TPS. Under the optimal conditions (the conditional optimization was shown in Figure S4), the ECL intensity exhibited a linear decrease with increasing concentrations of TPS from 2.5 pg/mL to 200 ng/mL (Figure 6A). The linear equation could be expressed as $\Delta E = 1198.6 \lg c + 9994.0$ (Figure 6B, here ΔE and c were the decreased ECL intensity and TPS concentrations, respectively), with the correlation coefficient of 0.993. The detection limit was calculated to be 0.81 pg/mL ($S/N = 3$), which was much lower than that of some existing methods. Comparing with the present proteins detection methods (Table S2), the sensor has a wide detection range and a high detection limit, indicating that it has excellent potential application in the clinical detection of proteins.

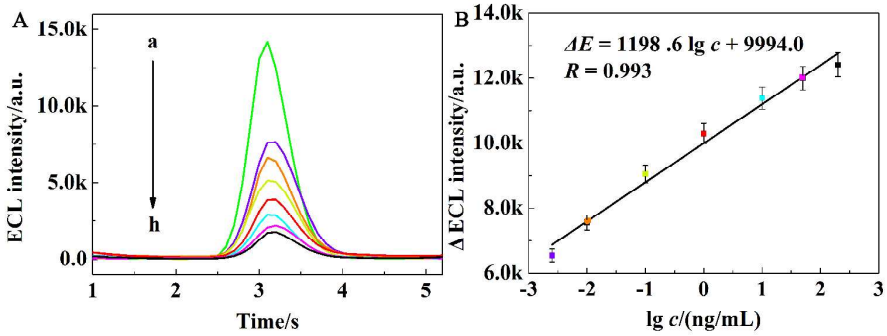

Figure 6. (A) ECL intensities of the ECL peptide-based biosensor for different concentrations of TPS detection in PBS (0.1 M, pH 8.0) (a-h). The concentrations of TPS: (a) 0 (b) 2.5 pg/mL, (c) 10 pg/mL, (d) 100 pg/mL, (e) 1 ng/mL, (f) 10 ng/mL, (g) 50 ng/mL, (h) 200 ng/mL. (B) Calibration curve for TPS determination.

Stability, selectivity and reproducibility of the ECL peptide-based biosensor. The stability of the proposed ECL peptide-based biosensor was monitored under continuous cyclic scans for 10 cycles at 50 ng/mL of TPS. The results were presented in Figure 7A, the ECL signals were almost unchanged, indicating the proposed biosensor has an excellent stability with relative standard deviation (RSD) of 0.8%.

Selectivity was another basic element for evaluating sensor performance. To investigate the selectivity of the proposed biosensor, PSA, AFP, CEA, TB and MMP-7 were chosen as interfering agents. Under the optimum experimental conditions, the 0.1 ng/mL of TPS solution containing 10 ng/mL of interfering substances were measured respectively. As can be seen from Figure 7B, there was no remarkable difference in ECL signal of mixed samples and that of PSA only, which indicating that the proposed ECL peptide-based biosensor has a good selectivity for PSA.

The reproducibility of the ECL peptide-based biosensor was determined by measuring the same TPS concentration (1 ng/mL) using five electrodes prepared under the same conditions (Figure 7C). The RSD was less than 5%, demonstrating that the reproducibility of the ECL biosensor was acceptable.

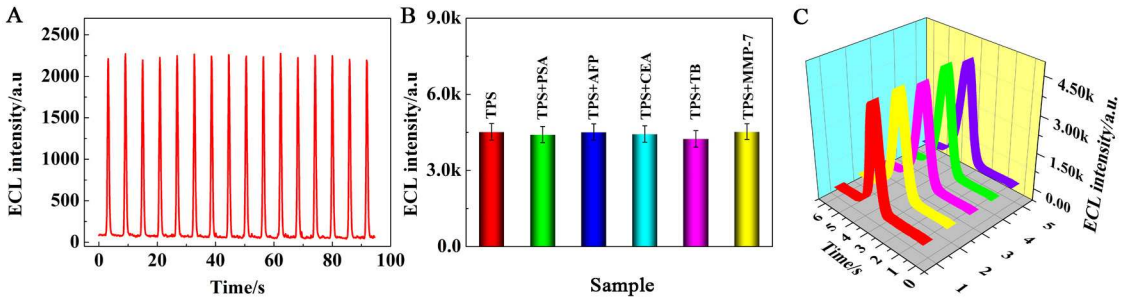

Figure 7. (A) Continuous cyclic potential scans of the proposed ECL peptide-based biosensor; (B) The ECL intensities response of the biosensors immersed in TPS (1 ng/mL) and TPS (1 ng/mL) with interferences (10 ng/mL), respectively. (C) The reproducibility of the ECL peptide-based biosensor.

Serum Sample Measurement. In order to further investigate the clinical application potential of the designed ECL peptide-based biosensor, a recovery experiment was conducted for detection of TPS by standard addition methods. First, the human serum (provided by Xinqiao Hospital of Chongqing) was 50-fold diluted by PBS (0.1 M, pH 8.0). Then, the serum was used to prepare the target (TPS) with different concentrations. At last, the prepared enzyme solution was incubated on the proposed electrode and the ECL intensity was tested. From the results presented in Figure S5, the linear equation of TPS detection in human serum was $E^* = 1157.9 \lg c^* + 10057.2$ (here ΔE^* and c^* were the decreased ECL intensity and TPS concentrations, respectively), which was similar to the -standard equation ($E = 1198.6 \lg c + 9994.0$). Moreover, the results of the recoveries listed in Table 1 (between 99.87% and 110.00%) were acceptable for TPS detection in real biological samples.

Table 1. Detection of TPS added in normal human serum with the proposed ECL peptide-based biosensor.

Sample number	ECL responses /(a.u.)	Added / (ng/mL)	Found / (ng/mL)	Recovery / %
1	5343.9	0.10	0.11	110.00
2	4179.6	1.00	1.03	103.00
3	2995.3	10.00	10.02	100.20
4	2159.1	50.00	49.95	99.90
5	1798.5	100.00	99.87	99.87

CONCLUSIONS

In conclusion, a highly sensitive ECL peptide-based biosensor for the detection of TPS has been demonstrated through AAPHNs as a co-reaction accelerator in the luminol-dissolved O_2 ECL system. The superior sensitive performance of the biosensor could be attributed to three aspects. First, we employed DNA nanotubes as carrier materials to efficiently immobilize luminol through the Dox-Lu composite structure, which could greatly increase the loading of luminol to achieve signal amplification. Second, AAPHNs as co-reaction accelerator, could effectively promote the ECL reaction between luminol and dissolve O_2 due to their unique geometrical shape and three-metal structures. Third, due to the target-induced cleavage strategy, the TPS act as not only the target, but also the enzyme to directly cleavage of VIP in the signal "on-off" switch system. In view of these advantages, the proposed ECL peptide-based biosensor exhibited remarkable accuracy, selectivity and stability, which may hold great significance in protein detection.

ASSOCIATED CONTENT

Supporting Information

The cleavage site of VIP, DNA sequences, the preparation process of AAPHNs, stepwise characterization of the sensing interface, comparison of the effect of different nanomaterials on the proposed biosensor, optimization of experimental

conditions, comparison of the proposed method with some reported methods for proteins detection, calibration curve of TPS detection in human serum. This information is available free of charge *via* the Internet at http://pubs.acs.org.

AUTHOR INFORMATION

*Tel.: + 86-23-68252277;

Fax: + 86-23-68253172.

E-mail address: yuanruo@swu.edu.cn (R. Yuan), yqchai@swu.edu.cn (Y. Q. Chai).

ACKNOWLEDGEMENTS

This work was supported by the NNSF of China (Grants 21775124, 21575116 21675129, and 51473136) and the Fundamental Research Funds for the Central Universities (Grant XDJK2016E055), China.

REFERENCES

(1) Qi, H.; Zhang, C.; Huang, Z.; Wang, L.; Wang, W.; Bard, A. J. *J. Am. Chem. Soc.* **2016**, *138*, 1947-1954.

(2) Shao, K.; Wang, B.; Ye, S.; Zuo, Y.; Wu, L.; Li, Q.; Han, H. *Anal. Chem.* **2016**, *88*, 8179-8187.

(3) Wang, Y. Z.; Hao, N.; Feng, Q. M.; Shi, H. W.; Xu, J. J.; Chen, H. Y. *Biosens. Bioelectron.* **2016**, *77*, 76-82.

(4) Dong, Y. P.; Zhou, Y.; Wang, J.; Zhu, J. J. *Anal. Chem.* **2016**, *88*, 5469−5475

(5). Yao, J.; Li, L.; Li, P.; Yang, M. *Nanoscale* **2017**, *9*, 13364-13383.

(6) Kitte, S. A.; Gao, W.; Zholudov, Y. T.; Qi, L.; Nsabimana, A.; Liu, Z.; Xu, G. *Anal. Chem.* **2017**, *89*, 9864-9869.

(7) Zhao, X.; Zhou, W.; Lu, C. *Anal. Chem.* **2017**, *89*, 10078-10084.

(8) Wu, L.; Ding, F.; Yin, W.; Ma, J.; Wang, B.; Nie, A.; Han, H. *Anal. Chem.* **2017**, *89*, 7578-7585.

(9) Hu, L. Z.; Xu, G. B.; *Chem. Soc. Rev*. **2010**, *39*, 3275-3304.

(10) Zhou, Y.; Wang, H. J.; Zhuo, Y.; Chai, Y. Q.; Yuan, R. *Anal. Chem.* **2017**, *89*, 3732-3738.

(11) Zhang, H. R.; Wu, M. S.; Xu, J. J.; Chen, H. Y. *Anal. Chem.* **2014**, *86*, 3834-3840.

(12) Jiang, X. Y.; Wang, Z.; Wang, H. J.; Zhuo, Y.; Yuan, R.; Chai, Y. Q. *Chem. Commun.* **2017**, *53*, 9705-9708.

(13) Ma, M. N.; Zhuo, Y.; Yuan, R.; Chai, Y. Q. *Anal. Chem*. **2015**, *87*, 11389_11397.

(14) Li, J. X.; Yang, L. X.; Luo, S. L.; Chen, B. B.; Li, J.; Lin, H. L.; Cai, Q. Y.; Yao, S. Z. *Anal. Chem.* **2010**, *82*, 7357-7361.

(15) Han, M.; Li, Y. R.; Niu, H. Y.; Liu, L. L.; Chen, K. J.; Bao, J. C.; Dai, Z. H.; Zhu, J. M. *Chem. Eur. J.* **2011**, *17*, 3739-3745.

(16) Wang, H. J.; Yuan, R.; Chai, Y. Q.; Cao, Y. L.; Gan, X. X.; Chen, Y. F.; Wang, Y. *Biosens. Bioelectron.* **2013**, *43*, 63-68.

(17) Xie, X.; Gao, G.; Kang, S.; Shibayama, T.; Lei, Y.; Gao, D.; Cai, L. *Adv. Mater*. **2015**, *27*, 5573-5577.

(18) Zhang, M. Q.; Timmerman, H. Mediat. *Inflamm.* **1997**, *6*, 311-317.

(19) Lavens, E.; Vanhage, H. M. *Forensic Sci. Int.* **1998**, *93*, 135-141.

(20) Fineschi, V.; Cecchi, R.; Centini, F. *Forensic Sci. Int.* **2001**, *120*, 189-194.

(21) Ayne, V.; Kam, P. *Anaesthesia* **2004**, *59*, 695-703.

(22) Sargur, R.; Cowley, D.; Murng, S. *Clin. Exp. Immunol*. **2011**, *163*, 339-345.

(23) Nikoobakht, B.; El-Sayed, M. A. *Chem. Mater*. **2003**, *15*, 1957-1962.

(24) Zhou, Y.; Zhuo, Y.; Liao, N.; Chai, Y. Q.; Yuan, R. *Talanta* **2014**, *129*, 219-226.

(25) Shi, X.; Chen, C.; Li, X.; Song, T.; Chen, Z.; Zhang, Z.; Wang, Y. *Soft Matter* **2015**, *11*, 8484-8492.

(26) He, H.; Du, J.; Hu, Y.; Ru, J.; Lu, X. *Talanta* **2013**, *115*, 381-385.

(27) Fennell, J.; He, D.; Tanyi, A. M.; Logsdail, A. J.; Johnston, R. L.; Li, Z. Y.; Horswell, S. L. *J. Am. Chem. Soc.* **2013**, *135*, 6554-6561.

(28) Toshima, N.; Yonezawa, T. *New J. Chem.* **1998**, *22*, 1179-1201.

(29) Jiang, Q.; Song, C.; Nangreave, J.; Liu, X. W.; Lin, L.; Qiu, D. L.; Wang, Z. G.; Zou, G. Z.; Liang, X. J.; Yan, H.; Ding, B. Q. *J. Am. Chem. Soc.* **2012**, *134*, 13396−13403.

(30) Xie, S. B.; Dong, Y. W.; Yuan, Y. L.; Chai, Y. Q.; Yuan, R. *Anal. Chem*. **2016**, *88*, 5218−5224.

(31) Dong, Y. P.; Wang, J.; Peng, Y.; Zhu, J. J. *Biosens. Bioelectron.* **2017**, *94*, 530-535.

(32) Cui, H.; Xu, Y.; Zhang, Z. F. *Anal. Chem.* **2004**, *76*, 4002-4010.

(33) Cui, H.; Zou, G. Z.; Lin, X. Q. *Anal. Chem.* **2003**, *75*, 324-331.

(34) Murthi, V. S.; Urian, R. C.; Mukerjee, S. *J. Phys. Chem. B* **2004**, *108*, 11011-11023.

(35) Wu, Y.; Wang, D.; Chen, X.; Zhou, G.; Yu, R.; Li, Y. *J. Am. Chem. Soc.* **2013**, *135*, 12220-12223.

(36) Zhang, Z.; Berg, A.; Levanon, H. *J. Am. Chem. Soc.* **2003**, *125*, 7959-7963.

for TOC only

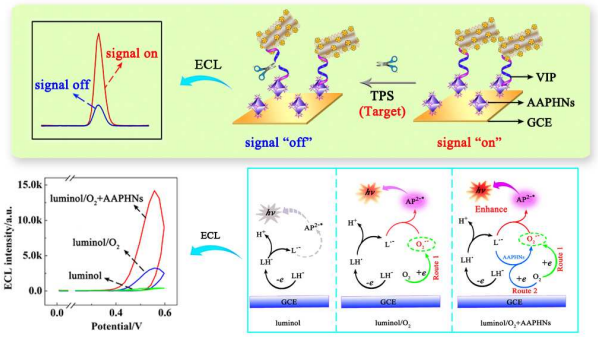
signal on
signal off
ECL
TPS
(Target)
VIP
AAPHNs
GCE
signal "off"
signal "on"
15.0k
10.0k
5.0k
0.0
ECL intensity/a.u.
luminol/O2+AAPHNs
luminol/O2
luminol
0.0
0.4
0.6
Potential/V
ECL
hv
Enhance
GCE
luminol
luminol/O2
luminol/O2+AAPHNs
Route 1
Route 2